Scripta Materialia 128 (2017) 53–56

Contents lists available at ScienceDirect

Scripta Materialia

journal homepage: www.elsevier.com/locate/scriptamat

Regular Article

Up-scaled solid state reaction for synthesis of doped Mg_2Si

Gwansik Kim [a], Hwijong Lee [a], Jeongmin Kim [a], Jong Wook Roh [a], Inwoong Lyo [b], Byung-Wook Kim [b], Kyu Hyoung Lee [c,*], Wooyoung Lee [a,*]

[a] Department of Materials Science and Engineering, Yonsei University, Seoul 03722, South Korea
[b] Advanced Materials Research Team, Central Advanced Research and Engineering Institute, Hyundai Motor Company, Uiwang 16082, South Korea
[c] Department of Nano Applied Engineering, Kangwon National University, Chuncheon 24341, South Korea

ARTICLE INFO

Article history:
Received 14 July 2016
Received in revised form 1 October 2016
Accepted 9 October 2016
Available online xxxx

Keywords:
Solid state reaction
Mg_2Si
Hot pressing
Spark plasma sintering
Reproducibility

ABSTRACT

Herein, we reported a synthesis technique based on the up-scaled solid state reaction for Al and Bi co-doped Mg_2Si polycrystalline bulks and investigated their thermoelectric transport properties. The powders (~1 kg/batch) were synthesized for mass production by using the solid state reaction, and the polycrystalline bulks were consolidated with a diameter of 25 mm and thickness of 3 mm using hot pressing and spark plasma sintering techniques. Both the hot pressed and the spark plasma sintered bulks showed good reproducibility and positional uniformity of the thermoelectric properties and the highest *ZT* value of 0.98 was obtained at 873 K.

1. Introduction

Recently, research on automotive thermoelectric generators (ATEGs) has made noticeable progress owing to the increasing CO_2 regulations and the interest in improving the fuel efficiency of vehicles. However, the development of high performance thermoelectric (TE) materials, which are evaluated by the dimensionless figure of merit *ZT* ($=\sigma S^2 T/\kappa_{tot}$, where σ is the electrical conductivity, *S* is the Seebeck coefficient, *T* is absolute temperature, and κ_{tot} is the total thermal conductivity), is a prerequisite for applications of ATEGs, since enhancement of the power generation efficiency is one of the most important factors in the commercialization of ATEGs.

Thus far, several materials have been studied for mid-temperature TE generators, and materials based on skutterudites, [1,2] half-Heusler alloys, [3,4] and silicides [5,6] have been found to be promising candidates for use in ATEGs. Among these materials, filled skutterudites and half-Heusler alloys provide a higher conversion efficiency (%) and power density (W/cm^2) in modules, [7,8] but their weight load and high production cost limit their application. In contrast, silicide-based materials are more attractive for ATEGs due to their relatively low density (~1.99 g/cm^3 for Mg_2Si) and the abundance of their elements on the Earth. However, their *ZT* values are still lower than those of filled skutterudites and half-Heusler alloys. Thus, recent studies on silicide-based TE materials have been focused on the enhancement of *ZT*. Among silicide-based TE materials, *n*-type Mg_2Si systems have been investigated intensively because they exhibit high electron mobility (possibility for high σ) and a conduction band with 2 subbands (possibility for large *S*) [9].

Several approaches including engineering of the compositions or microstructures have been proposed to enhance the *ZT* of Mg_2Si. Substitutional doping for compositional tuning has been widely used to enhance the power factor (σS^2) by modified density of states (DOS) and/or reduced the lattice thermal conductivity ($\kappa_{lat} = \kappa_{tot} - \kappa_{ele}$, where κ_{ele} is electronic thermal conductivity) by intensified phonon scattering. Sn is a well-established *Si*-site substitutional dopant, and Sn-doped Mg_2Si compounds exhibit enhanced $ZT > 1.0$ owing to the synergetic effects of band convergence and point defect phonon scattering [10,11]. Recently, very high *ZT* values over 1.2 were obtained in doped $Mg_2Si_{1-x}Sn_x$ through the nontraditional processing technologies such as melt spinning and pressure-less SPS, [12,13] however, $Mg_2Si_{1-x}Sn_x$ solid solutions are easily decomposed into the Sn-rich and Si-rich phases at high temperatures (>773 K) [14]. Bi is also known as an effective Si-site dopant that simultaneously enhances the power factor (enlarged DOS) and reduces κ_{lat} by phonon scattering (point defect formation), and Bi-doped Mg_2Si exhibits high $ZT > 0.6$ [15,16]. In a previous report, it was experimentally demonstrated that Al (Mg-site) and Bi (Si-site) are effective dopants for Mg_2Si. We fabricated Al and Bi co-doped Mg_2Si polycrystalline bulks using solid state reaction followed by spark plasma sintering (SPS), and observed significantly enhanced *ZT* of approximately 1.02 at 873 K in

* Corresponding authors.
E-mail addresses: khlee2014@kangwon.ac.kr (K.H. Lee), wooyoung@yonsei.ac.kr (W. Lee).

http://dx.doi.org/10.1016/j.scriptamat.2016.10.010
1359-6462/

$Mg_{1.96}Al_{0.04}Si_{0.97}Bi_{0.03}$. Co-doping of Al and Bi enhanced the power factor as a result of the increased DOS effective mass (m_d^*) and the reduced κ_{lat} by point defect phonon scattering [17].

However, well-defined fabrication processes for Mg_2Si-based TE materials are necessary for mass production owing to the evaporation of Mg during the melting or heat treatment for formation of solid solutions. Mg_2Si-based TE powders are usually synthesized by solid state reaction, [18] melting, [19] mechanical alloying, [20] and flux method [21]. Among these methods, the solid state reaction is a simple and scalable process for large-scale fabrication of powders and has an advantage in the preparation of compounds composed of elements with large differences in the melting points. However, the drawback associated with the solid state reaction is the difficulty in synthesizing powders without secondary phases, suggesting that sufficient reaction time is required during the sintering process.

In the present study, we fabricated 1 kg/batch scale powders of $Mg_{1.96}Al_{0.04}Si_{0.97}Bi_{0.03}$ using two-step solid state reaction technique and evaluated the TE transport properties of polycrystalline bulks compacted by SPS and hot pressing (HP). By optimization the solid state reaction and sintering conditions, we demonstrated good reproducibility (~6%, batch to batch) and positional uniformity (~8%) of the TE properties and obtained high *ZT* value of 0.98 at 873 K for HPed $Mg_{1.96}Al_{0.04}Si_{0.97}Bi_{0.03}$.

2. Experiment

Fig. 1 shows a schematic diagram of the solid state reaction for 1 kg/batch powders of $Mg_{1.96}Al_{0.04}Si_{0.97}Bi_{0.03}$. The weighed starting elemental powders (STEP 1) of Mg (99.8%, Alfa Aesar), Si (99.9%, Alfa Aesar), Al (99.5%, Alfa Aesar), and Bi (99.999%, Alfa Aesar) were mixed in stoichiometric amounts using conventional ball milling (STEP 2). 5 wt.% of Mg was added to compensate for Mg evaporation during the solid state reaction process. The mixed powders were pressed into disks of diameter 30 mm (~6.25 g) under 40 MPa (STEP 3). 16 cold pressed disks (~100 g) were put into an alumina crucible (STEP 4), which was covered with a quartz tube to prevent contamination by vaporized Mg (STEP 5). Finally, 10 quartz tubes were stacked in an alumina tube installed in a furnace (STEP 6). The solid state reaction for formation of the solid solution was performed by 2-step heat treatment. The first step was conducted by heating at 673 K for 1 h under vacuum atmosphere, and then at 823 K for 1 h, and the temperature was maintained for 6 h. The acquired samples were pulverized into powders using a conventional ball mill for 24 h, and separated by sieving to obtain particles with diameters smaller than 53 μm.

The disc-type compacted bulks (25 mm in diameter and 3 mm in thickness) were fabricated using SPS (1023 K for 5 min under 70 MPa) and HP (1023 K for 60 min under 70 MPa) and their relative densities ranged from 97% to 99% of the theoretical density. The X-ray diffraction (XRD) method (Ultima IV/ME 200DX, Rigaku, Japan) with CuKα radiation was used to characterize the phase formation behavior of the samples, and the lattice constants were calculated using Rietveld refinement. The temperature dependence of electronic transport properties σ and S was measured using a commercial instrument (ZEM-3, ULVAC, Japan) from 300 K to 873 K. The κ_{tot} values were obtained using the equation $\kappa_{tot} = \rho_s C_p \lambda$, where ρ_s is the density, C_p is the specific heat capacity, and λ is the thermal diffusivity. The λ and C_p values with temperature were measured using the laser flash method (Netzsch LFA-457, Germany) under vacuum and differential scanning calorimetry (DSC 8000, Perkin Elmer, USA), respectively. The Hall effect was measured under a 1 T magnetic field in the van der Pauw configuration, and the carrier concentration (n_c) and carrier mobility (μ_{Hall}) were estimated by using the one-band model. The microstructure of the samples was obtained using a scanning electron microscope (SEM, JEOL-7800F, JEOL Ltd., Japan).

3. Results and discussion

To evaluate the reproducibility of the TE properties, we fabricated 10 pellets (batch to batch samples) using powders obtained from each alumina crucible. We also prepared 5 samples from each pellet, as shown in the inset of Fig. 3(a), to investigate the positional uniformity. Fig. 2 shows the XRD patterns and lattice constants of $Mg_{1.96}Al_{0.04}Si_{0.97}Bi_{0.03}$, which was cut from the middle of pellets sintered by SPS (SPS_3) and HP (HP_3). All major patterns are indexed antifluorite structures with the cubic Fm3m space group, and the MgO and Bi_2Mg_3 secondary phases are identified in both the SPSed and the HPed samples. It should be noted that the contents of Bi_2Mg_3 largely decreased in HP_3, indicating that the solubility of Bi would be increased by HP due to the longer reaction time. The average contents of Bi_2Mg_3 for SPSed and HPed $Mg_{1.96}Al_{0.04}Si_{0.97}Bi_{0.03}$ are ~9.7 wt.% and ~1.7 wt.%, respectively. This is clearly observed in the XRD patterns and the variation in the lattice constants, as shown in Fig. 2(b) and (c). The 2θ of the (220) peak for HP_3 is lower than that for SPS_3, indicating that the lattice constant is increased by the substitution of Bi with a larger ionic radius than that of Si. As shown in Fig. 2(c), the lattice constant of HP_3 (~6.369 Å) is larger than that of SPS_3 (~6.357 Å).

The increased solubility of Bi by HP is also verified from the electronic transport data because the solubility of Bi at the Si-site intrinsically affects the electronic and thermal transport properties of Mg_2Si-based compounds. As shown in Fig. 3(a), the σ values of the HPed samples are much higher (~55%) than those of the SPSed samples in the whole measured temperature range. This is considered to be related with the increase of Bi solubility. To clarify this, we measured the Hall effect at 300 K and calculated the n_c and μ_{Hall} and represented them in Table 1. The average n_c value (~1.20×10^{20} cm^{-3}) of HPed samples (HP_1–HP_5) was 41% higher compared with that of the SPSed ones (~8.49×10^{19} cm^{-3}, SPS_1–SPS_5), due to the increased donor-like Bi solubility. This sensitivity of n_c values ranged from 8.5×10^{19} cm^{-3} (SPSed $Mg_2Si_{0.97}Bi_{0.03}$) to 1.69×10^{20} cm^{-3} (HPed $Mg_2Si_{0.97}Bi_{0.03}$) with fabrication process related with the actual Bi-doping contents was reported in previous studies [15,22,23]. The μ_{Hall} value (~98.9 cm^2 V^{-1} s^{-1}) of the HPed samples was also higher than that of the SPSed ones

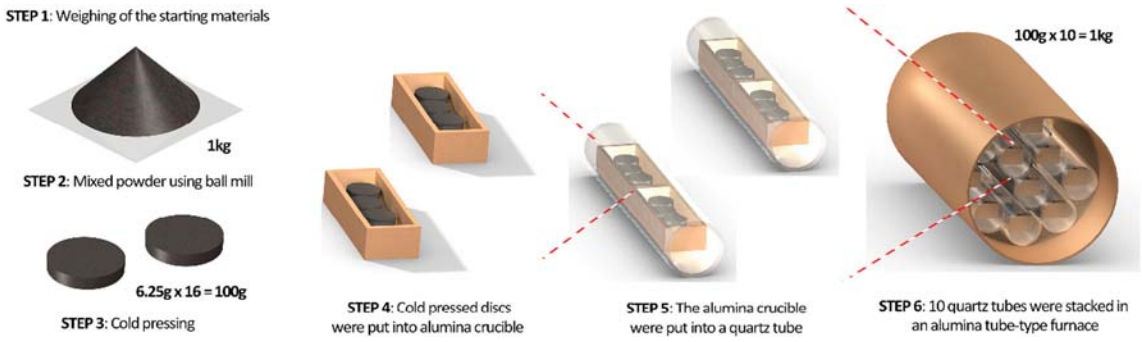

Fig. 1. Schematic diagram of solid state reaction for 1 kg/batch powders of $Mg_{1.96}Al_{0.04}Si_{0.97}Bi_{0.03}$.

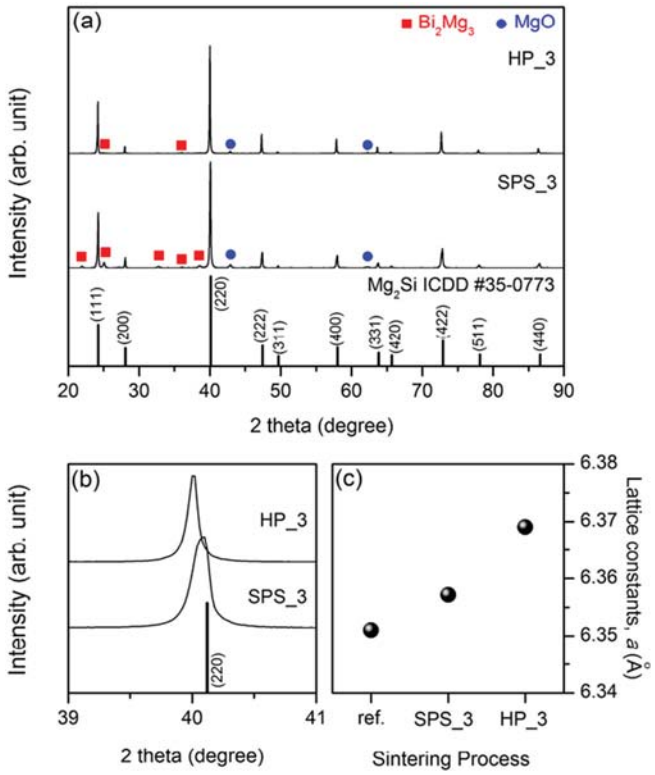

Fig. 2. (a, b) XRD patterns and (c) the variation in lattice constants for HP_3 and SPS_3 $Mg_{1.96}Al_{0.04}Si_{0.97}Bi_{0.03}$ samples.

(~84.1 $cm^2 V^{-1} s^{-1}$), suggesting that the electron scattering was significantly reduced by a decrease in impurities, as shown in Fig. 2(a). Another possible reason for the higher μ_{Hall} of the HPed samples might be related with the microstructure. The SEM images of the fractured surface of SPSed and HPed samples are presented in Fig. 4. The average grain size of the HPed sample is ~8 μm, while that of the SPSed sample is ~3 μm owing to the short sintering time, however, μ_{Hall} would not be significantly deteriorated by electron scattering at the grain boundaries in both samples considering electron mean free paths of Mg_2Si (<20 nm) [24]. Meanwhile, the S values of the SPSed and HPed samples exhibited a trade-off relation with σ (inset of Fig. 3(b)). The calculated power factor (Fig. 3(b)) values of the HPed samples were higher than those of the SPSed sampled owing to the optimized n_c by the increased Bi solubility. The maximum power factor value of ~3.38 mW $m^{-1} K^{-2}$ at 773 K was obtained for HP_3.

To elucidate the reproducibility of our fabrication technique, the variations in TE properties among the batch to batch samples were evaluated. As shown in Fig. 3(a) and (b), the ranges of error bars for the electronic transport properties of the SPSed and HPed pellets are ~5% in σ, ~2% in S, and ~6% in the power factor. We also investigated the positional uniformity by separate measurement for 5 samples cut from a pellet (inset of Fig. 3(a)). Both the SPSed and HPed samples show similar values of deviation (~6% in σ, ~3% in S, and ~8% in the power factor) with respect to the positions. These results suggest that our up-scaled solid state reaction based synthesis technique was very feasible for mass production of doped Mg_2Si.

On the other hand, despite the higher σ, the κ_{tot} values of HPed samples (2.87 W $m^{-1} K^{-1}$ at 873 K for HP_3) are almost the same as those of the SPSed ones (2.89 W $m^{-1} K^{-1}$ at 873 K for SPS_3) as shown in the inset of Fig. 3(c). To elucidate this, κ_{lat} values are estimated by subtracting the electronic contribution (κ_{ele}), which is calculated using the Wiedemann–Franz law ($\kappa_{ele} = L\sigma T$), from the κ_{tot} values. We adopted Lorentz numbers (L) of 2.31 × 10^{-8} $V^2 K^{-2}$ for HP_3 and

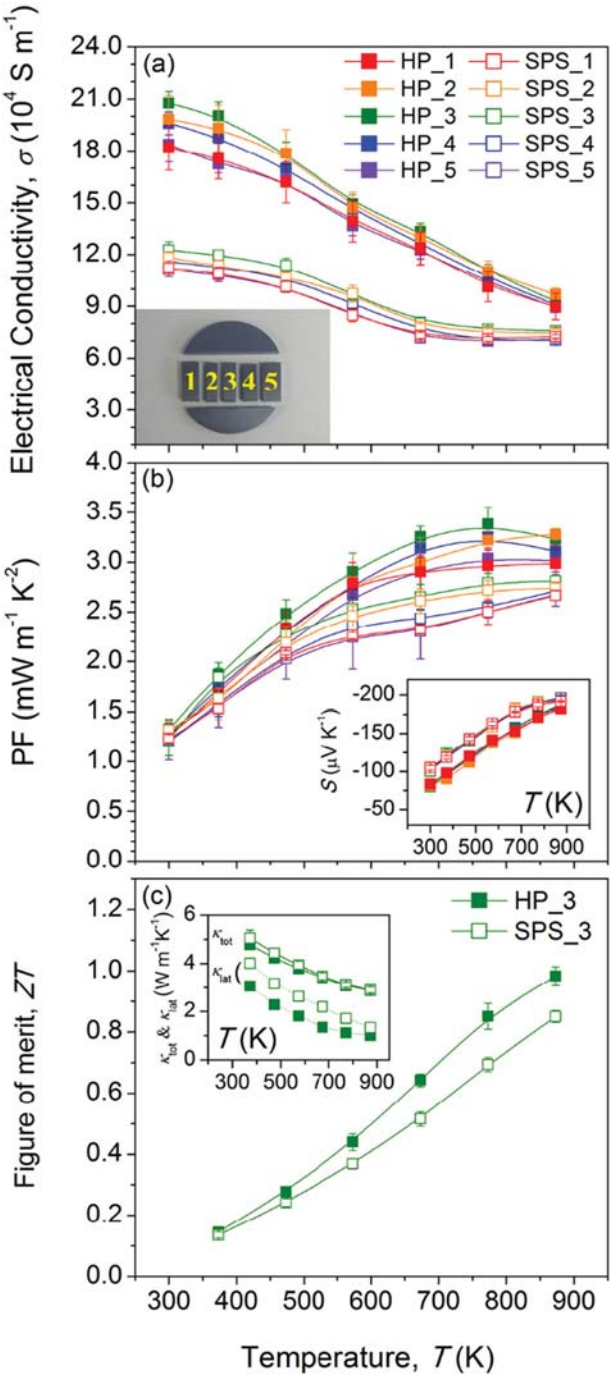

Fig. 3. Temperature dependence of (a) electrical conductivity, (b) power factor, and (c) ZT for HPed and SPSed $Mg_{1.96}Al_{0.04}Si_{0.97}Bi_{0.03}$ samples. The insets of (a), (b), and (c) show the photo of 5 samples cut from a pellet, Seebeck coefficient, and total and lattice thermal conductivity, respectively.

2.36 × 10^{-8} $V^2 K^{-2}$ for SPS_3 approximated from following equation [25]:

$$L = \left(\frac{k_B}{e}\right)^2 \left(\frac{(r+{}^7/_2)F_{r+{}^5/_2}(\eta)}{(r+{}^3/_2)F_{r+{}^1/_2}(\eta)} - \left[\frac{(r+{}^5/_2)F_{r+{}^3/_2}(\eta)}{(r+{}^3/_2)F_{r+{}^1/_2}(\eta)}\right]^2 \right)$$

where r is the scattering parameter, $F_n(\eta)$ is the n-th order Fermi integral, and η is Fermi energy, respectively. The κ_{lat} values of HP_3 (3.06 W $m^{-1} K^{-1}$ at 300 K and 1.00 W $m^{-1} K^{-1}$ at 873 K) are much lower than those of SPS_3 (4.00 W $m^{-1} K^{-1}$ at 300 K and

Table 1
Room temperature electronic transport parameters for HPed and SPSed $Mg_{1.96}Al_{0.04}Si_{0.97}Bi_{0.03}$ samples.

	σ (S m^{-1})	S (μV K^{-1})	n_c (cm^{-3})	μ_{Hall} (cm^2 V^{-1} s^{-1})	Density (%)
$Mg_{1.96}Al_{0.04}Si_{0.97}Bi_{0.03}$_SPS_1	112,250.97	−104.80	7.90×10^{19}	87.3	98.63
$Mg_{1.96}Al_{0.04}Si_{0.97}Bi_{0.03}$_SPS_2	118,223.36	−105.57	8.80×10^{19}	82.6	98.91
$Mg_{1.96}Al_{0.04}Si_{0.97}Bi_{0.03}$_SPS_3	122,596.24	−99.78	9.27×10^{19}	81.4	99.53
$Mg_{1.96}Al_{0.04}Si_{0.97}Bi_{0.03}$_SPS_4	115,871.79	−102.13	8.53×10^{19}	83.5	99.02
$Mg_{1.96}Al_{0.04}Si_{0.97}Bi_{0.03}$_SPS_5	111,182.63	−104.06	7.96×10^{19}	85.9	98.48
$Mg_{1.96}Al_{0.04}Si_{0.97}Bi_{0.03}$_HP_1	181,719.88	−83.33	1.12×10^{20}	99.7	98.04
$Mg_{1.96}Al_{0.04}Si_{0.97}Bi_{0.03}$_HP_2	198,329.91	−81.40	1.26×10^{20}	97.1	98.48
$Mg_{1.96}Al_{0.04}Si_{0.97}Bi_{0.03}$_HP_3	207,642.12	−79.91	1.27×10^{20}	100.2	98.84
$Mg_{1.96}Al_{0.04}Si_{0.97}Bi_{0.03}$_HP_4	195,967.16	−80.53	1.25×10^{20}	96.5	98.56
$Mg_{1.96}Al_{0.04}Si_{0.97}Bi_{0.03}$_HP_5	183,731.61	−83.16	1.12×10^{20}	101.0	98.30

1.33 W m^{-1} K^{-1} at 873 K) in whole measure temperature range, indicating the intensified point defect phonon scattering owing to the increased Bi solubility of HPed samples. The possible mechanisms for phonon scattering are mass difference and strain by the contrast of atomic radius between the host Si (M_{Si} ~ 28.1; r_{Si} ~ 110 pm) and dopant Bi (M_{Bi} ~ 208.9; r_{Bi} ~ 160 pm). The evaluated ZT values of SPS_3 and HP_3 from measured the σ, S, and κ_{tot} are represented in Fig. 3(c). Owing to the synergetic effects of the power factor enhancement by n_c optimization and κ_{lat} reduction by phonon scattering promotion, the ZT value of HP_3 was significantly enhanced and reached a maximum value of 0.98 at 873 K.

4. Conclusions

A simple and scalable synthesis technique was developed for doped Mg_2Si compounds based on combination of solid state reaction and hot pressing. Up-scaled powders of $Mg_{1.96}Al_{0.04}Si_{0.97}Bi_{0.03}$ were prepared by a 2-step solid state reaction process, and highly dense polycrystalline bulks were fabricated using spark plasma sintering and hot pressing. We found that a sufficient sintering time is required to obtain high-purity solid solution bulks when the large-scale powders of doped Mg_2Si are synthesized by the solid state reaction. Compared with the spark plasma sintered samples, the hot pressed samples exhibited enhanced the electronic and thermal transport properties owing to the long reaction time, thus increasing the Bi solubility at the Si-sites. Moreover, we realized good reproducibility and uniformity of the thermoelectric properties, which is one of the most important factors for commercialization of thermoelectric power generation systems.

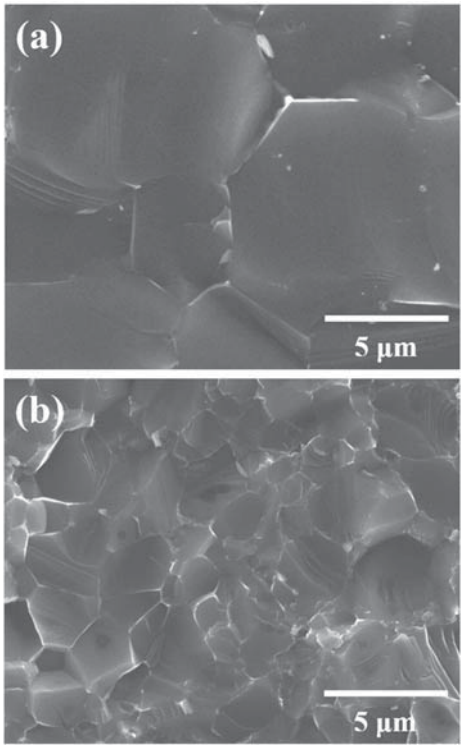

Fig. 4. SEM images of the fractured surface of (a) HP_3 and (b) SPS_3 $Mg_{1.96}Al_{0.04}Si_{0.97}Bi_{0.03}$ samples.

Acknowledgements

This work was supported by Hyundai Motor Company (2015-11-0146), the National Research Foundation of Korea (NRF) Grant funded by the Korea government (MSIP) (2014R1A2A1A10053869), the Priority Research Centers Program (2009-0093823), and the Industrial Fundamental Technology Development Program (10052977) funded by the Ministry of Trade, Industry and Energy (MOTIE) of Korea.

References

[1] B.C. Sales, D. Mandrus, R.K. Williams, Science 272 (1996) 1325–1328.
[2] G.S. Nolas, M. Kaeser, R.T. Littleton IV, T.M. Tritt, Appl. Phys. Lett. 77 (2000) 1855–1857.
[3] C. Uher, J. Yang, S. Hu, D.T. Morelli, G.P. Meisner, Phys. Rev. B 59 (1999) 8615–8621.
[4] Q. Shen, L. Chen, T. Goto, T. Hirai, J. Yang, G.P. Meisner, C. Uher, Appl. Phys. Lett. 79 (2001) 4165–4167.
[5] V.K. Zaitsev, M.I. Fedorov, E.A. Gurieva, I.S. Eremin, P.P. Konstantinov, A.Y. Samunin, M.V. Vedernikov, Phys. Rev. B 74 (2006) 045207.
[6] J. Tani, H. Kido, Intermetallics 15 (2007) 1202–1207.
[7] K. Salzgeber, P. Prenninger, A. Grytsiv, P. Rogl, E. Bauer, J. Electron. Mater. 39 (2010) 2074–2978.
[8] H. Xie, H. Wang, Y. Pei, C. Fu, X. Liu, G.J. Snyder, X. Zhao, T. Zhu, Adv. Funct. Mater. 23 (2013) 5123–5130.
[9] W. Liu, X.J. Tan, K. Yin, H.J. Liu, X.F. Tang, J. Shi, Q.J. Zhang, C. Uher, Phys. Rev. Lett. 108 (2012) 166601.
[10] X. Liu, T. Zhu, H. Wang, L. Hu, H. Xie, G. Jiang, G. Snyder, X. Zhao, Adv. Energy Mater. 3 (2013) 1238–1244.
[11] X. Zhang, H. Liu, S. Li, F. Zhang, Q. Lu, J. Zhang, Mater. Lett. 123 (2014) 31–34.
[12] H. Ning, G.D. Mastrorillo, S. Grasso, B. Du, T. Mori, C. Hu, Y. Xu, K. Simpson, G. Maizza, M.J. Reece, J. Mater, Chem. A 3 (2015) 17426–17432.
[13] X. Zhang, H. Liu, Q. Lu, J. Zhang, F. Zhang, Appl. Phys. Lett. 103 (2013) 063901.
[14] Q. Zhang, Y. Zheng, X. Su, K. Yin, X.F. Tang, C. Uher, Scr. Mater. 96 (2015) 1–4.
[15] J. Tani, H. Kido, Physica B 364 (2005) 218–224.
[16] S.K. Bux, M.T. Yeung, E.S. Toberer, G.J. Snyder, R.B. Kaner, J.P. Fleurial, J. Mater. Chem. 21 (2011) 12259–12266.
[17] G. Kim, J. Kim, H. Lee, S. Cho, I. Lyo, S. Noh, B.W. Kim, S.W. Kim, K.H. Lee, W. Lee, Scr. Mater. 116 (2016) 11–15.
[18] W. Liu, Q. Zhang, K. Yin, H. Chi, X. Zhou, X. Tang, C. Uher, J. Solid State, Chem. 203 (2013) 333–339.
[19] M. Søndergaard, M. Christensen, K.A. Borup, H. Yin, B.B. Iversen, Acta Mater. 60 (2012) 5745–5751.
[20] S.W. You, K.H. Park, I.H. Kim, S.M. Choi, W.S. Seo, S.U. Kim, J. Electron. Mater. 41 (2012) 1675–1679.
[21] H. Gao, T. Zhu, X. Liu, J. Mater. Chem. 21 (2011) 5933–5937.
[22] M. Ioannou, G.S. Polymeris, E. Hatzikraniotis, K.M. Paraskevopoulos, T. Kyratsi, J. Phys, Chem. Solids 75 (2014) 984–991.
[23] N. Farahi, M. VanZant, J. Zhao, J.S. Tse, S. Prabhdev, G.A. Botton, J.R. Salvador, F. Borondics, Z. Liu, H. Kleinke, Dalton Trans. 43 (2014) 14983–14991.
[24] N. Satyala, D. Vashaee, Appl. Phys. Lett. 100 (2012) 073107.
[25] L.D. Zhao, S.H. Lo, J.Q. He, H. Li, K. Biswas, J. Androulakis, C.I. Wu, T.P. Hogan, D.Y. Chung, V.P. Dravid, M.G. Kanatzidis, J. Am. Chem. Soc. 133 (2011) 20476–20487.